

# Determination of the electron effective mass of 2D electrons in AlGa<sub>N</sub>/AlN/GaN heterostructure by Raman-scattering measurements

ENGİN TIRAS

*Department of Physics, Faculty of Science, Anadolu University, Yunus Emre Campus, 26470 Eskisehir, Turkey*

The electron effective mass in AlGa<sub>N</sub>/AlN/GaN heterostructure grown by the metalorganic chemical vapor deposition (MOCVD) technique was determined from the phonon–plasmon coupled-mode line-shape analysis of vibrational spectroscopy measurements. The vibrational properties of AlGa<sub>N</sub>/AlN/GaN heterostructures were studied using Raman scattering spectroscopy at room temperature. 532 nm (2.33 eV) was used as the excitations in the Raman scattering measurement. The effective mass obtained from the Raman scattering spectroscopy is in good agreement with the current results in the literature.

(Received May 2, 2012; accepted September 20, 2012)

*Keywords:* GaN heterostructure, Raman spectra, Electron effective mass, Phonon–plasmon coupled-mode

## 1. Introduction

The III-N and III-V-N are ideal materials for the construction of blue/green light-emitting devices (LEDs and lasers) and high electron mobility transistors that are intended to operate at high power and high temperatures because of their wide band gap structure [1].

Despite the progress in the development of devices, many fundamental material parameters of AlGa<sub>N</sub>/AlN/GaN are still not fully understood. The knowledge on these parameters, such as effective mass of electrons, is important for the exploration and optimization of this material system in device applications. Determination of the effective mass of electrons, under the environmental conditions in the steady state, provides useful information about the electron–phonon interactions. Furthermore, electron–phonon scattering processes determine the high-field transport phenomena in semiconductors and thus form the basis for many ultrafast optoelectronic devices. The field of electron–phonon scattering processes in semiconductors thus provides a link between fundamental semiconductor physics and high-speed devices. The effective mass of electrons in many semiconductors is also affected from the environmental conditions such as temperature, magnetic field, electrical field, light intensity. Therefore, it needs to be determined the effective mass of electrons from different experimental techniques. There are three main techniques used in the evaluation of the transport properties of materials, namely, magnetotransport, cyclotron resonance absorption under high magnetic field and Raman spectroscopy.

To date, many experimental work reported effective masses of AlGa<sub>N</sub>/GaN structure that were obtained from the analysis of magnetotransport [2-4], cyclotron resonance [5-6], and both of these techniques'

measurements [7-8]. Due to small electron mobility, it is difficult to obtain the 2D electron effective mass from magnetoresistance measurements. Experimentally evaluated electron effective mass in AlGa<sub>N</sub>/GaN as a function of the two-dimensional electron gas density formed at the interface of an AlGa<sub>N</sub>/GaN heterostructure with different alloy composition was summarized by *Kurakin et al* [4]. They found the electron effective mass in AlGa<sub>N</sub>/GaN to be independent of the electron concentration. This result for the effective mass of 2D electrons was in good agreement with the bulk effective mass in GaN where effective mass was reported [4, 9] to be  $0.2 \pm 0.02 m_0$  ( $m_0$  is the free electron mass).

Raman scattering is a non-destructive technique to characterize crystal quality. In addition, Raman scattering by longitudinal-optic-phonon-plasmon-coupled (LOPC) mode measurements are commonly used to determine the effective mass and carrier concentration in III-N [10-13], III-V [14-21] and III-V-N semiconductors [22, 23] by using the Drude, hydrodynamical, and Lindhard-Mermin models. The mechanisms for light scattering in the theoretical approach play an important role. The deformation potential associated with the allowed electro-optic, charge density fluctuation, and forbidden Flöhlich light scattering mechanisms are usually considered in these calculations [17].

In this work, electron effective mass in AlGa<sub>N</sub>/AlN/GaN heterostructures is determined by using Raman measurements. The experimental Raman LOPC mode results are compared with analytical expressions of the Drude and Lindhard-Mermin models. The results are discussed in the framework of the current theoretical models concerning electron effective mass in semiconductors.

## 2. Experimental

The AlGaN/AlN/GaN heterostructure was grown by the metalorganic chemical vapor deposition (MOCVD) technique. Standard trimethylgallium (TMGa), trimethylaluminum (TMAI), trimethylindium (TMIn) and ammonia (NH<sub>3</sub>) were used as the precursors for Ga, Al, In and N, respectively. During the growth, the sample parameters including doping density, alloy fractions, and layer thicknesses were estimated from the calibrated charts for the specific growth conditions and materials. The sample was grown on c-face (0001) sapphire (Al<sub>2</sub>O<sub>3</sub>) substrates. Before initiating the epitaxial growth, substrates were subjected to a heat process under a nitrogen environment at 1100 °C in order to clean oxides on the surface for 10 min. The growth process started with the growth of a 320 nm thick AlN buffer layer was grown at 1150 °C. A 1700 nm thick undoped GaN template layer was grown at 1050 °C. To reduce the penetration of the electron wave function to the barrier layer and hence alloy scattering, an approximately 1 nm thick AlN spacer layer was grown at 1150 °C. Then, an AlGaN barrier layer of 20 nm thick was grown over the spacer layer at 1050 °C. The AlGaN layer was also doped with Si, doping density 10<sup>18</sup> cm<sup>-3</sup>. The growth process was finished with a 3 nm thick GaN cap layer at 1050 °C. After the growth, these parameters were measured for each wafer, using standard characterization techniques such as atomic force microscope, ellipsometry capacitance-voltage profiling, and energy dispersive x-ray analysis [24]. The 2D electron gas was formed at the interface between the undoped GaN layer and AlN spacer. The layer structure of the sample is shown in Table 1.

Table 1. Layer structure of the AlGaN/AlN/GaN heterostructure sample.

Layer	Thickness (nm)
GaN (cap layer)	3
AlGaN	20
AlN (spacer layer)	1
GaN (undoped)	1700
AlN (buffer layer)	320
Sapphire (substrate)	

The Raman spectra were obtained at room temperature by using the Bruker Optics FT-Raman Scope III system. As an excitation source, a wavelength of 532 nm (2.33 eV) was applied in the sample growth direction (*c*-axis). A 50x objective is used. Extreme care is taken to avoid sample damage or laser induced heating. Measurements are performed from 20 to 0.2 mW incident power. No significant spectral change is observed in this range.

## 3. Results and discussions

Fig. 1 shows the room-temperature Raman for AlGaN/AlN/GaN heterostructures recorded in the grown-axis backscattering configurations ( $z(xx)\bar{z}$ ). In our sample, GaN crystallizes in a wurtzite structure whose *z*-axis is perpendicular to the sapphire substrate plane. The space group is  $C_{6v}^4$  and the  $A_1(\text{LO})$  and  $E_2$  modes are allowed in this configuration [25]. There is a sharp and strong peak at 573.5 cm<sup>-1</sup>, known as the non-polar high frequency  $E_2$  mode, which implies the strong correlation between Ga and N atoms on the *c*-plane [14, 26]. The polar vibrations  $A_1$  observed at 738.5 cm<sup>-1</sup> correspond to a correlation between Ga and N atoms. Since the light penetration depth of 532 nm is longer than the thickness of the coated wafer on the sapphire substrate, the sapphire origin  $A_{1g}$  and  $E_g$  modes were observed at approximately 421 (also at 658 cm<sup>-1</sup>) and 753 cm<sup>-1</sup>, respectively. Although the contribution to the vibration modes that implies the correlation between Ga and N atoms is caused by both GaN cap layer and undoped GaN layer where 2D electron gas formed, the main source of the peak intensities may come from undoped GaN layer where excess free carrier concentration.

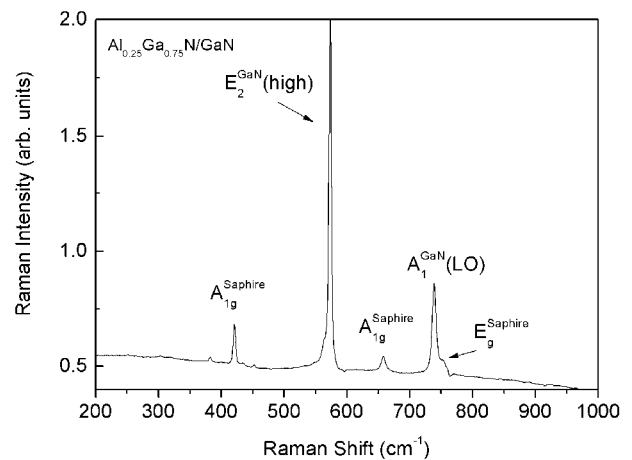


Fig. 1. Raman spectra in AlGaN/AlN/GaN heterostructure.

The scattering mechanisms that affected to the Raman spectra intensity play an important role. At high temperatures polar optical phonon scattering is dominant in GaN [27]. In this perspective, it has been shown that the three-dimensional (3D) approach to polar optical-phonon scattering is justifiable for the 2DEG (Refs [28-30]). Therefore, 3D approach to Raman scattering line shape fitting analysis is justifiable for 2D electron gas. A similar method has been used also for InGaAsN/GaAs single quantum wells [22].

In order to simulate the Raman scattering line shapes for plasmon-related excitations, it is considered the dielectric function [12, 14-17, 19, 31]:

$$\varepsilon(q, \omega) = \varepsilon_\infty + 4\pi(\chi_i + \chi_e). \quad (1)$$

The first term on the right-hand side of eq. (1) is the high-frequency dielectric constant which refers to the contribution of the background,

$$\chi_i(\omega) = \frac{\varepsilon_\infty}{4\pi} \frac{\omega_{LO}^2 - \omega^2}{\omega_{TO}^2 - \omega^2 - i\Gamma\omega} \quad (2)$$

is the polar lattice contribution to the susceptibility, and  $\chi_e$  is the free-carrier contribution to the susceptibility,  $\omega$  is the scattering light frequency,  $\Gamma$  is the phonon anharmonic

damping constant,  $\omega_{TO}$  and  $\omega_{LO}$  are the frequencies of the transverse and longitudinal optical phonons, respectively. According to the Drude model, the  $\chi_e$  term is described by

$$\chi_e(\omega) = -\frac{\varepsilon_\infty}{4\pi} \frac{\omega_p^2}{\omega(\omega + i\gamma_p)}, \quad (3)$$

where  $\gamma_p$  ( $=e/\mu_H m^*$ ) is the collision frequency of the free charge carriers in which  $e$  is the electron charge and  $m^*$  is the electron effective mass,  $\omega_p$  ( $=4\pi N_e e^2 / \varepsilon_\infty m^*$ ) is the plasma frequency in which  $N_e$  is the 3D carrier concentration [31]. In the Drude model, the intensity of Raman scattering under the deformation potential and electro-optic mechanism is given by

$$I(\omega) \propto \text{Im} \left\{ -\frac{1}{\varepsilon(q, \omega)} \left[ \frac{\varepsilon_\infty}{4\pi} + 2 \frac{\omega_{TO}^2}{\omega_{LO}^2 - \omega_{TO}^2} C \chi_i - \left( \frac{\omega_{TO}^2}{\omega_{LO}^2 - \omega_{TO}^2} C \right)^2 \chi_i \left[ 1 + \frac{4\pi}{\varepsilon_\infty} \chi_e \right] \right] \right\} \quad (4)$$

where  $C$  is the Faust-Henry coefficient [17, 19, 31].

The Raman scattering intensity is also examined by Lindhard-Mermin model. In this model, scattering mechanisms that contributed to the intensity is assumed to be independent of each other. The deformation potential associated with the allowed electro-optic (DP+EO), charge density fluctuation (CDF), and forbidden Flöhlich (IFF) mechanisms are widely used in these calculations [27]. In the Lindhard-Mermin model, the Raman scattering intensity equation is given by [12, 17, 18, 20]:

$$I(\omega) \propto S(\omega) \text{Im} \left\{ -\frac{1}{\varepsilon(q, \omega)} \right\} \quad (5)$$

where function  $S(\omega)$  depends on the scattering mechanisms [41]. For the deformation potential associated

with the allowed electro-optic (DP+EO) scattering mechanism, the function  $S(\omega)$  is given by [14, 17]

$$S(\omega) = 1 + 2C \frac{\omega_{TO}^2}{\Delta} \left[ \omega_p^2 \gamma_p (\omega_{TO}^2 - \omega^2) + \omega^2 \Gamma (\omega_p^2 - \gamma_p^2 - \omega^2) \right] + C^2 \frac{\omega_{TO}^4}{\Delta (\omega_{LO}^2 - \omega_{TO}^2)} \left\{ \omega_p^2 [\gamma_p (\omega_{LO}^2 - \omega_{TO}^2) + \Gamma (\omega_p^2 - 2\omega^2)] + \omega^2 \Gamma (\omega^2 + \gamma_p^2) \right\} \quad (6)$$

With

$$\Delta = \omega_p^2 \gamma_p \left[ (\omega_{TO}^2 - \omega^2)^2 + \omega^2 \Gamma^2 \right] + \omega^2 \Gamma (\omega_{LO}^2 - \omega_{TO}^2) (\omega^2 + \gamma_p^2) \quad (7)$$

For the charge density fluctuation (CDF) mechanism, the function  $S(\omega)$  is given by [17]

$$S(\omega) = q^2 \left[ \frac{\omega_p^2}{\Delta} \gamma_p (\omega_{LO}^2 - \omega^2)^2 + \omega_p^4 \Gamma^2 (\omega_{LO}^2 - \omega_{TO}^2)^2 + \gamma_p \Gamma^2 \omega^2 \omega_p^2 \right]. \quad (8)$$

The contribution of the allowed electro-optic (DP+EO) scattering mechanism in GaN is large when compared to those of the charge density fluctuation (CDF) mechanism [14]. For the numerical calculation of the Raman scattering intensity, the phonon frequencies ( $\omega_{TO}=533 \text{ cm}^{-1}$ ,  $\omega_{LO}=735 \text{ cm}^{-1}$ ), Faust-Henry coefficient ( $C=0.4$ ) and high frequency dielectric constant ( $\varepsilon_\infty=5.35$ ) values of GaN given in Ref. 26 have been used. In the theoretical calculation, the phonon anharmonic damping constant ( $\Gamma$ ) has a significant effect on the amplitude and width of the  $A_1(\text{LO})$  peak rather than peak position.

So, it has been taken as  $\Gamma=8.2 \text{ cm}^{-1}$  for the best amplitude and width peak shape. For the  $N_e$ , and  $\gamma_p$  ( $=211 \text{ cm}^{-1}$ ), the room temperature low-field Hall Effect measurements sheet electron concentration value ( $N_e=2 \times 10^{17} \text{ cm}^{-3}$ ) and room temperature Hall mobility value ( $\mu_H=1325 \text{ cm}^2/\text{V.s}$ ) have been used, respectively [32].

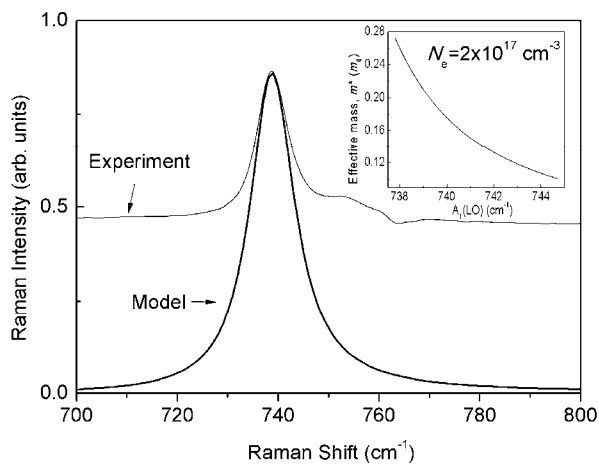


Fig. 2. Experimental evaluated Raman spectra near  $A_1(LO)$  and calculated line shapes of the LO mode. Inset:  $A_1(LO)$  frequency dependence of the calculated effective mass for  $N_e=2 \times 10^{17} \text{ cm}^{-3}$ .

Both the Lindhard-Mermin model and the Drude model were used in the calculations and the peak position of the  $A_1(LO)$  is found to be same. The calculated results are shown in Fig. 2. Effective mass of 2D electrons in AlGaIn/GaN heterostructures is found to be  $m^*=0.206m_0$  and this value is exactly the same as determined from the SdH measurements [33]. The  $A_1(LO)$  mode observed in AlGaIn/GaN heterostructures is particularly sensitive to variations in  $m^*$  which decrease with increasing  $A_1(LO)$  mode frequency. The calculated  $A_1(LO)$  mode frequency versus effective mass at constant sheet electron concentration is also shown inserted graph in figure 2. This result demonstrates that a change in  $A_1(LO)$  mode frequency has measurable effects on the effective mass, and hence that the analysis of the Raman spectra can provide useful information about  $m^*$  in AlGaIn/GaN heterostructures. The determined electron effective mass agrees with that obtained by other research groups [12] for AlGaIn/GaN heterostructures with the same aluminum mole fraction.

## 5. Conclusions

The electron effective mass in AlGaIn/GaN heterostructures can be determined by means of optical technique. The analysis of the LOPC mode Raman line shape based on the Lindhard-Mermin and Drude models allow the effective mass to be determined from fits to the experimental Raman spectra. The results obtained from Raman spectra are in good agreement with the results of Shubnikov de Haas effect results. These results constitute an independent and definite validation of the reliability of Raman scattering as a tool for contactless effective mass determinations in semiconductors.

## Acknowledgements

This work is supported by the Anadolu University under the project BAP-1001F99 and TUBITAK under the Project 110T377. I would like to thank to E. Ozbay, and S.B. Lisesivdin for growing the samples, and J. Ibanez for useful discussions on the topic. I also acknowledge the support of COST Action: MP0805 for providing a suitable platform for the successful execution of this research.

## References

- [1] S. Nakamura, S. J. Pearton, G. Fasol, *The Blue Laser Diode: the complete story* (Springer 2000)
- [2] S. Elhamri, R.S. Newrock, D.B. Mast, M. Ahoujja, W.C. Mitchel, J.M. Redwing, M.A. Tischler, J.S. Flynn, *Phys. Rev. B* **57**, 1374 (1998).
- [3] A. Saxler, P. Debray, R. Perrin, S. Elhamri, W.C. Mitchel, C.R. Elsass, I.P. Smorchkova, B. Heying, E. Haus, P. Fini, J.P. Ibbetson, S. Keller, P.M. Petroff, S.P. DenBaars, U.K. Mishra, J.S. Speck, *J. Appl. Phys.* **87**, 369 (2000).
- [4] A.M. Kurakin, S.A. Vitusevich, S.V. Danylyuk, H. Hardtdegen, N. Klein, Z. Bougrioua, A.V. Naumov, A. E. Belyaev, *J. Appl. Phys.* **105**, 073703 (2009).
- [5] Y.J. Wang, R. Kaplan, H.K. Ng, K. Doverspike, D.K. Gaskill, T. Ikedo, I. Akasaki, H. Amono, *J. Appl. Phys.* **79**, 8007 (1996).
- [6] S. Syed, J.B. Heroux, Y.J. Wang, M.J. Manfra, R.J. Molnar, H.L. Stormer, *Appl. Phys. Lett.* **83**, 4553 (2003).
- [7] W. Knap, E. Frayssinet, M.L. Sadowski, C. Skierbiszewski, D. Maude, V. Falko, M. Asif Khan, M.S. Shur, *Appl. Phys. Lett.* **75**, 3156 (1999).
- [8] Z.-F. Li, W. Lu, S.C. Chen, S. Holland, C.M. Hu, D. Heitmann, B. Shen, Y.D. Zheng, T. Someya, Y. Arakawa *Appl. Phys. Lett.* **80**, 431 (2001).
- [9] I. Vurgaftman, J. R. Meyer, L. R. Ram-Mohan, *J. Appl. Phys.* **89**, 5815 (2001).
- [10] M. Ramsteiner, J. Wagner, P. Hiesinger, K. Köhler, U. Rössler, *J. Appl. Phys.* **73**, 5023 (1993).
- [11] S. Ernst, A.R. Goni, K. Syassen, M. Cardona *Phys. Rev. B* **53**, 1287 (1996).
- [12] L. Artus, R. Cusco, J. Ibanez, N. Blanco, G. Gonzalez-Diaz, *Phys. Rev. B* **60**, 5456 (1999).
- [13] R. Cusco, L. Artus, J. Ibanez, N. Blanco, G. Gonzalez-Diaz, M. Rahman, A.R. Long, *J. Appl. Phys.* **88**, 6567 (2000).
- [14] T. Kozawa, T. Kachi, H. Kano, Y. Taga, M. Hashimoto, *J. Appl. Phys.* **75**, 1098 (1994).
- [15] M. Ramsteiner, O. Brandt, K.H. Ploog, *Phys. Rev. B* **58**, 1118 (1998).
- [16] J. S. Thakur, D. Haddad, V. M. Naik, R. Naik, G.W. Auner, H. Lu, W.J. Schaff, *Phys. Rev. B* **71**, 115203 (2005).

- [17] F. Demangeot, C. Piquier, J. Frandon, M. Gaio, *Phys. Rev. B* **71**, 104305 (2005).
- [18] J.M. Pomeroy, M. Kuball, C.H. Swartz, T.H. Myers, H. Lu, W.J. Schaff, *Phys. Rev. B* **75**, 035205 (2007).
- [19] R. Cusco, E. Alarcon-Llado, J. Ibanez, T. Yamaguchi, Y. Nanishi, L. Artus, *J. Phys.: Condens. Matter* **21**, 415801 (2009).
- [20] V. Yu. Davydov, A. A. Klochikhin, A. N. Smirnov, I. Yu. Strashkova, A.S. Krylov, H. Lu, W. J. Schaff, H. M. Lee, Y.L. Hong, S. Gwo, *Fiz. Tekh. Poluprovodn.* 44, [Semicond. 44 161] 170 (2010).
- [21] J.G. Kim, Y. Kamei, N. Hasuike, H. Harima, K. Kisoda, K. Sasamoto, A. Yamamoto, *Phys. Stat. Solidi C* **7-8**, 1887 (2010).
- [22] P. A. Grandt, A. E. Griffith, M. O. Manasreha, D. J. Friedman, S. Dogan, D. Johnstone, *Appl. Phys. Lett.* **85**, 4905 (2004).
- [23] J. Ibanez, R. Cusco, E. Alarcon-Llado, L. Artus, A. Patane, D. Fowler, L. Eaves, K. Uesugi, I. Suemune, *J. Appl. Phys.* **103**, 103528 (2008).
- [24] E. Arslan, S. Butun, Y. Safak, H. Uslu, I. Tascioglu, S. Altindal, E. Ozbay, *Microelectron. Reliability* **51**, 370 (2011).
- [25] T. Azuhata, T. Sota, K. Suzuki, and S. Nakamura, *J. Phys. Condens. Matter* **7**, L129 (1995).
- [26] I. M. Tiginyanu, A. Sarua, G. Irmer, J. Monecke, S. M. Hubbard, D. Pavlidis, V. Valiev, *Phys. Rev. B* **64**, 233317 (2001).
- [27] S.B. Lisesivdin, N. Balkan, O. Makarovsky, A. Patane, A. Yildiz, M.D. Caliskan, M. Kasap, S. Ozelik, E. Ozbay, *J. Appl. Phys.* **105**, 093701 (2009).
- [28] B. L. Gelmont, and M. Shur, M. Sroscio, *J. Appl. Phys.* **77**, 657 (1995).
- [29] L. Hsu, W. Walukiewicz, *Phys. Rev. B* **56**, 1520 (1997).
- [30] Y. Li, Y. Zhang, and Y. Zeng, *J. Appl. Phys.* **109**, 073703 (2011).
- [31] G. Abstreiter, M. Cardona, and A. Pinczuk, in: M. Cardona, G. Güntherodt (Eds.), *Light Scattering in Solids IV, Topics in Applied Physics*, vol. 54 (Springer, Berlin, 1984)
- [32] O. Celik, E. Tiras, S. Ardali, S. B. Lisesivdin, E. Ozbay, *Cent. Eur. J. Phys.* **10**, 485 (2012).
- [33] O. Celik, E. Tiras, S. Ardali, S. B. Lisesivdin, E. Ozbay, *Phys. Status Solidi C* **8**, 1625 (2011).

---

Corresponding author: etiras@anadolu.edu.tr